3.3 COUPLED ATMOSPHERE-FIRE MODELING AND FIRE BEHAVIOR SENSITIVITY TO ATMOSPHERIC INSTABILITY

Mary Ann Jenkins[†*]
York University, Toronto, Canada

1. INTRODUCTION

Two parameters believed to be particularly important in influencing wildfire evolution and structure are lower–level atmospheric stability and moisture.

Observational studies (e.g., Brotak & Reifsnyder 1977; Werth & Ochoa 1993; Potter 1996, etc.) provide evidence of a relationship between unstable environmental lapse rates, dry air, and large or erratic fire growth. Several of these studies investigated correlations between the level of wildfire risk and the Haines Index (Haines 1988), an operational fire–weather index based on the stability and moisture content of the near-surface atmosphere. Using the Clark et al (1996a,b) coupled wildfire–atmosphere numerical prediction model, Coen and Clark (2000) described the complex interactions between a wildfire and the atmosphere in an environment forced by terrain, low–level atmospheric stability, and vertical wind shear. None of these studies, however, isolated the effects of near-surface atmospheric stability and/or humidity on wildfire behavior. If we are to use the Haines Index accurately to predict wildfire behavior, it is important to understand exactly what are the effects of environmental atmospheric stability on wildfire behavior.

The purpose of this study is to investigate, through comparative numerical simulations with the Clark et al (1996a,b) model, the sensitivity of wildland fires to atmospheric stability, and in the process explore the dependence between atmospheric stability, wildfire behavior, and the Haines Index. Four different numerical fire experiments are presented. Two of the fire experiments correspond to Haines Indexes for low and moderate potential for severe fire development. The other two fire experiments correspond to the Haines Index for high potential for severe fire development.

* *Corresponding author address:* Mary Ann Jenkins, York University, Dept. of Earth and Atmospheric Science, 4700 Keele Street, Toronto, Ontario, Canada M3J 1P3; maj@yorku.ca

† *Additional affiliation:* Visiting Associate Professor, Department of Meteorology, 135 S 1460 E, University of Utah, Salt Lake City, Utah, USA 84112-0110; mjenkins@met.utah.edu

The Taylor diagram (Taylor, 2001) is introduced and used to evaluate how closely certain model field variables match each other in terms of their correlation, root–mean–square difference, and ratio of their variances. The advantage of the Taylor diagram, compared to simply reporting these statistics for each field variable being examined, is that the information is plotted on a single diagram.

For the objectives of this study, the Clark et al (1996a,b) model is coupled with the Canadian Forest Service Fire Behavior Prediction System or FBPS (Hirsch 1996). Clark et al's simple ignition tracer parameterization has been replaced. The forest fuel is divided into rectangular grids. To trace ignition in the current model, four tracers, assigned to each model fuel cell, identify burning areas and define the fire front within fuel cells. The coordinates of the ignition tracers are time dependent and allow fires of arbitrary orientation and shape to move through a mesh of fuel grids at fire–spread rates directed by the fire–scale winds. The tracers move normal to the model wind at the fire spread-rate formula based on the FBPS. The tracer advecting wind and therefore spread rates are prescribed at the height of 15 m above ground level, which represents the top of the forest canopy.

TABLE 1. Description of the Haines Indexes for each numerical experiment, where B is the difference between the dry bulb and dew point temperatures at 85 kPa, A is the temperature lapse between 95 and 85 kPa, and the Haines Index = $a + b$.

Experiment	A (°C)	a	B (°C)	b
a1b3/t01q15	1	1	15	3
a2b3/t06q15	6	2	15	3
a3b3/t11q15	11	3	15	3
a3b3/t08q11	8	3	11	3

2. LOW-ELEVATION HAINES INDEX

The Haines Index is calculated by adding a temperature term a to a moisture term b. For fires at low elevation, values from 1 to 3 are assigned to a based

on the temperature lapse between 95 and 85 kPa. For fires at low elevation, values from 1 to 3 are assigned to b based on the difference between the dry bulb and dew point temperatures at 85 kPa. The Haines Index varies from 2 to 6. A Haines Index of 2 indicates moist, stable air, and the potential for large fire growth or extreme fire behavior is very low. A Haines Index of 6 indicates dry, unstable air, and the potential for large fire growth or extreme fire behavior is high. The higher the Haines Index, the more likely that the fire behavior is severe.

Table 1 shows the temperature and moisture limits used to compute four different low–elevation Haines Indexes for the four numerical experiments of this study. In the first three experiments, B = 15 °C and the moisture term $b = 3$, indicating dry air. The difference between the three Haines Indexes depends on a, where $a + b = 4$, 5, and 6 designates the potential for large fire growth or extreme fire behavior as low, moderate, and high, respectively. Based on the A and B values, experiment a3b3/t11q15 is at the top of the range for the Haines Index, i.e., about the largest values prescribed by Haines (1988) to a high–risk fire. In the fourth experiment, a3b3/t08q11, the Haines Index is 6, but in this case both A and B are lowest values that Haines (1988) prescribes to a high–risk fire.

3. EXPERIMENTAL SET-UP

With the exception of experiment a3b3/t11q15, one level of mesh refinement with two–way interactive grid nesting was used in the simulations. An inner fire domain, 1.2 km^2 in size, was nested within an outer domain, 6 km^2 in size. The horizontal resolutions were $\Delta x = \Delta y = 150$ m in the outer domain and $\Delta x = \Delta y = 50$ m in the inner fire domain. The near–surface vertical resolutions were $\Delta z = 40$ m in the outer domain and $\Delta z = 20$ m in the inner domain. The horizontal resolution of the fuel grid was $\Delta x_{\rm fuel} = \Delta y_{\rm fuel} = 25$ m. The time resolutions were $\Delta t = 1$ s in the outer domain and $\Delta t = 1/3$ s in the inner domain. Preliminary model runs showed that for experiment a3b3/t11q15, it was necessary to add a third and larger outer domain, 18 km^2 in size, to ensure that the fire domain was not contaminated by outer boundary disturbances. Horizontal resolutions were $\Delta x = \Delta y = 450$ m and $\Delta t = 3$ s in the outermost domain. The 50 m grid size in the fire domain allowed simulations of significant duration to track the evolution of the model fire and yet was able to resolve the important larger–scale features associated with fire behavior.

TABLE 2. Description of mixing ratio r, temperature T, and dew–point temperature T_d at pressure P levels 100, 95, and 85 kPa for each experiment.

Experiment	P (kPa)	r (g/kg)	T (°C)	T_d (°C)
a1b3/t01q15	100	11.76	27.0	16.4
	95	6.93	22.6	7.7
	85	7.29	21.6	6.8
a2b3/t06q15	100	11.76	27.0	16.4
	95	6.93	22.6	7.7
	85	5.09	16.6	1.7
a3b3/t11q15	100	11.76	27.0	16.4
	95	6.93	22.6	7.7
	85	3.42	11.6	-3.3
a3b3/t08q11	100	11.76	27.0	16.4
	95	9.07	22.6	11.7
	85	5.85	14.6	3.7

The experiments started with a spot fire of radius three times the hypotenuse of a fuel cell. There was no Coriolis force and no topography. The model environmental wind was initially set to a constant westerly 3 m s^{-1}. Table 2 shows each of the four experiment's mixing ratio (r g kg^{-1}), temperature (T °C), and dew–point temperature (T_d °C) prescribed at the surface pressure P of 100 kPa and pressure levels 95 kPa and 85 kPa. Surface pressure, mixing ratio, and temperature were the same for all experiments, and surface relative humidity was 50%. Above 85 kPa (approximately 550 m) to a tropopause of 10 km, water vapor decayed exponentially to a minimum of 0.1 g kg^{-1}, and the buoyancy frequency was 0.01 s^{-1}. Above the tropopause to the top of the outer domain (approximately 13 km), the buoyancy frequency was 0.02 s^{-1}. The fire model specifications are similar to those in Clark et al (1996a,b), except that the ground and canopy fuels were homogeneous and equal combinations of Spruce, mature Jack Pine, and immature Jack Pine, and the fire spread-rate formula was based on the FBPS.

The upper–air and surface fields chosen for examination are: u, the x or east–west wind component; v, the y or north–south wind component, w, the z or vertical wind component; P, the pressure perturbation (defined as the deviation from background or environmental pressure profile); B, the buoyancy (as in Clark et al 1996a,b); Q, the q_v water vapor mixing ratio; V_x, the x vorticity component; V_y, the y vorticity component; V_z, the z vorticity component; Sh, the vertical wind shear;

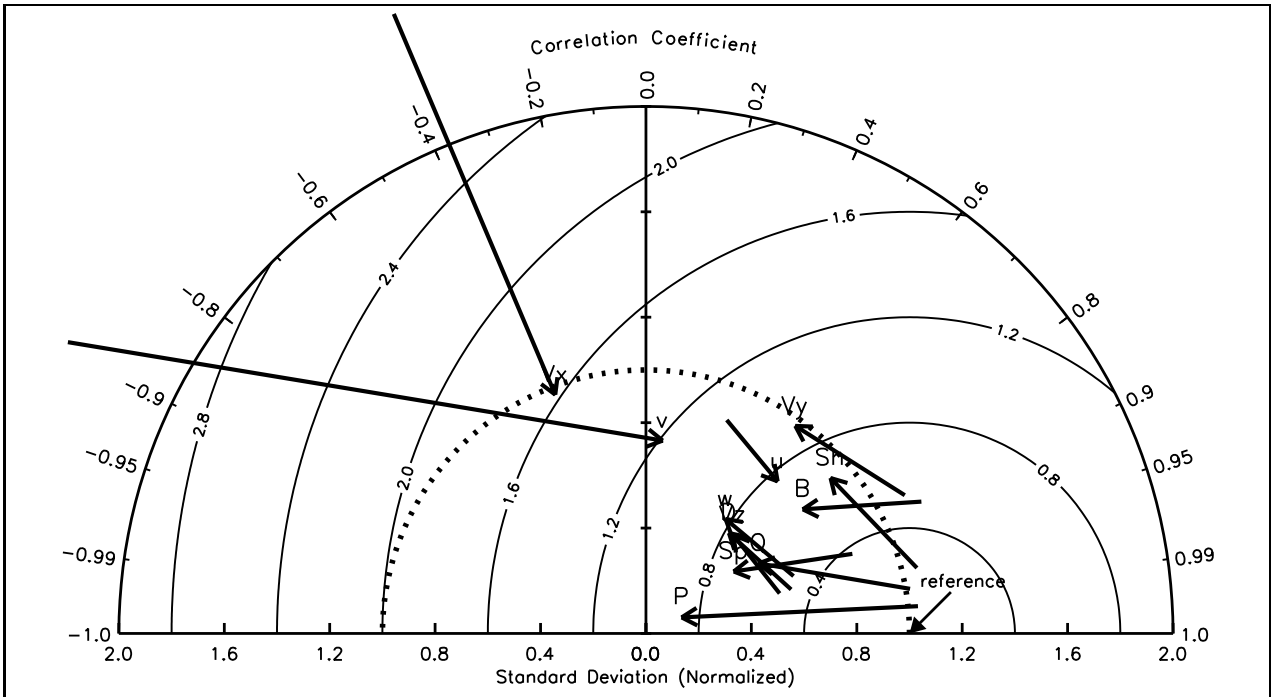

Fig. 1 Changes in pattern statistics between experiments a2b3/t06q15 and a3b3/t08q11. Statistics for experiment a2b3/t06q15 are plotted at the tails of arrows, and statistics for experiment a3b3/t08q11 are plotted at the heads of arrows. The RMS error and standard deviations are normalized by the standard deviation of each field from the reference experiment a1b3/t01q15 before plotting. The fields shown are: u, the x or east–west wind component; v, the y or north–south wind component, w, the z or vertical wind component; P, the pressure perturbation; B, the buoyancy; Q, the q_v water vapor mixing ratio; V_x, V_y, and V_z, the x, y, and z, vorticity components, respectively; Sh, the vertical shear; Sp, the horizontal wind speed; and D, the horizontal convergence. For each field, the data were sampled every 5 seconds between a 4 to 3600 second time period, at 15 m above ground level, and averaged over the burning area.

Sp, the horizontal wind speed; and D, the horizontal divergence. The surface–only fields chosen for examination are: CI, CL, CS, the intensity, latent heating rate, and sensible heating rate, from the canopy burn; GI, GL, GS, the intensity, latent heating rate, and sensible heating rate, from the surface fuel burn; SR, the fire spread rate.

Each experiment was run for two hours, and model field data were output every 4 seconds. Averages of each field over the unburned area, burning area, and the total fire domain area were calculated, and the minimum and maximum field values within the fire domain were determined. The Taylor plots were made using the averages over the burning area and are presented next.

4. RESULTS

By recognizing a simple geometrical relationship between four statistical quantities — the correlation coefficient, the pattern root–mean–square (RMS) difference E', and the standard deviations σ_f and σ_r — Taylor (2001) constructed a two–dimensional plot that quantifies the degree of similarity between fields f and r, where the four statistical quantities are indicated by a single point. The radial distance from the plot's origin is proportional to the standard deviation of a pattern. The RMS difference between f, the "test" field, and r, the "reference" field, is proportional to their distance apart (in the same units as the standard deviation). The correlation between the two fields is given by the azimuthal position of the f field. The correlation coefficient indicates how much difference is due to structure and phase, and the standard deviations indicate the difference in the amplitude of the variations from the mean for r and f.

A comparison between three experiments is made in each Taylor diagram. The Taylor statistics for each field selected for analysis (previous section) quantify the correspondence between the three experiments. Two of the experiments are chosen as test experiments and one as the reference ex-

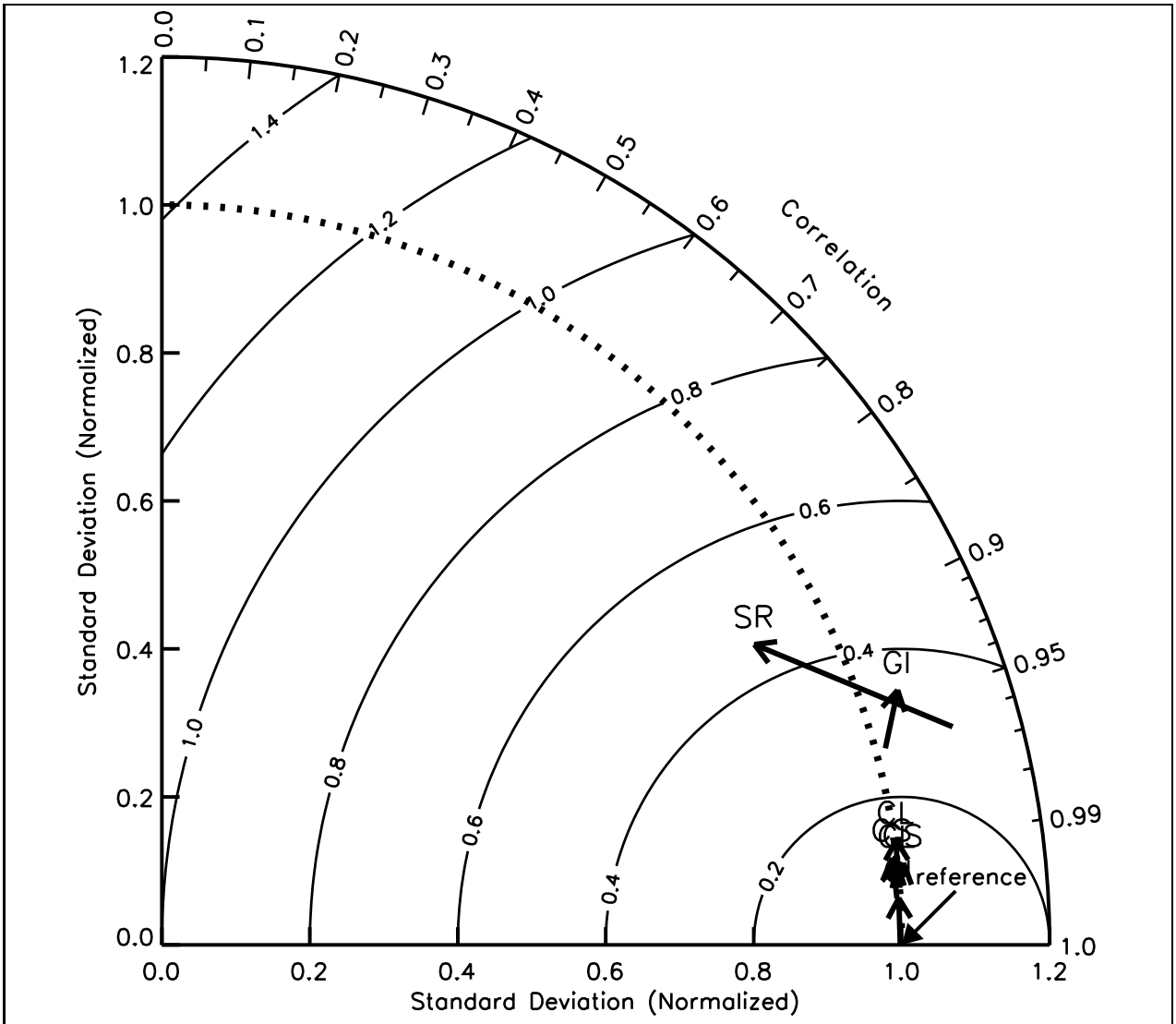

Fig. 2 Changes in normalized pattern statistics between experiments a2b3/t06q15 and a3b3/t08q11. Statistics for experiment a2b3/t06q15 are plotted at the tails of arrows, and the statistics for experiment a3b3/t08q11 are plotted at the heads of arrows. The RMS error and standard deviations are normalized by the standard deviation of each field from the reference experiment a1b3/t01q15 before plotting. The fields shown are: CI, CL, CS, the intensity, latent heating rate, sensible heating rate, from the canopy burn; GI, GL, GS, the intensity, latent heating rate, sensible heating rate, from the ground fuel burn; and SR, the fire spread rate. For each field, the data were sampled every 5 seconds between a 4 to 3600 second time period, at 0 m above ground level and averaged over the burning area.

periment. Two points connected by an arrow are plotted for each field. The tail of the arrow indicates the statistics for the first test experiment, the head of the arrow indicates the statistics for the second test experiment. Because the units of measure are different for each field, their statistics are non–dimensionalized before appearing on the same graph. For each variable, the pattern RMS difference and the standard deviation are normalized by the standard deviation of the corresponding reference field r (i.e., $\widehat{E}' = E'/\sigma_r$, $\widehat{\sigma}_f = \sigma_f/\sigma_r$, $\widehat{\sigma}_r = 1$). The correlation coefficient is unchanged, and the final statistics yield a normalized Taylor diagram. The standard deviation of the reference field is normalized by itself, and is plotted a unit distance from the origin along the abscissa. For our purposes, experiment a1b3/t01q15 is the reference experiment, and experiments a2b3/t06q15,

a3b3/t08q11, and a3b3/t11q15 are the tests. The RMS error and standard deviations are normalized by the standard deviation of each field from model fire a1b3/t01q15 before plotting. From this point on, all references to RMS are to *normalized* pattern RMS differences, and all references to standard deviations are to *normalized* variances or standard deviations. Since there was significant variation in the evolution of each fire within the first hour of simulation, model data from this time period were used to produce the Taylor statistics and plots. The model data were sampled at 5 s time intervals and at a single height level, either at the surface, or at 15 m above ground level, the top of the canopy.

a. Experiments a2b3/t06q15 and a3b3/t08q11 compared to a1b3/t01q15

Fig. 1 shows the Taylor statistics based on averages over the burning area for experiments a1b3/t01q15, a2b3/t06q15, and a3b3/t08q11. Except for u, v, and V_x, fields from experiment a2b3/t06q15 lie relatively close to the reference point. The RMS differences (tails of arrows) are relatively small (less than or approximately equal to 0.5) and the correlation coefficients between these fields and the reference field are greater than 0.8. The standard deviations of fields B, P, Q, Sh, and V_y are near 1.0, while the standard deviations of fields w, V_z, Sp, and D show an overall *reduction* in the amplitude of the variations compared to that of the reference ($\widehat{\sigma}_f < 1$). Fields Q, P, and Sh not only have the same amplitude of variations compared to the reference, but are nearly completely in phase.

Fig. 1 shows the fields from experiment a2b3/t06q15 that have changed most compared to the reference are u, v, and V_x. The RMS difference of 1.07 for u is due primarily to the poor correlation or phase difference (0.35) and not the difference in the amplitude of variations ($\widehat{\sigma}_f \approx 0.9$). The RMS difference of 3.06 for V_x is due to a poor and negative correlation or phase difference (-0.4) combined with a moderately large difference in the amplitude of variations ($\widehat{\sigma}_f \approx 2.5$). The RMS difference of 3.4 for v is due to a good but negative correlation (-0.9) and a moderately large difference in the amplitude of the variations ($\widehat{\sigma}_f \approx 2.5$).

Fig. 1 also shows the Taylor statistics of experiment a3b3/t08q11 (heads of arrows) compared to the reference experiment. Except for u, v, and V_x, the RMS differences for experiment a3b3/t08q11 are greater than the RMS differences for experiment a2b3/t06q15 (the head of the arrow lies further away from the reference point than the tail). The arrows are oriented such that the variances are *smaller* in experiment a3b3/t08q11 compared to experiment a2b3/t06q15, and the correlations between experiment a3b3/t08q11 (rated as a low–end Haines Index 6) and the reference are even further reduced compared to those of experiment a2b3/t06q15 (rated as a Haines Index 5) and the reference. For these fields the RMS differences are greater than 0.6 and less than or equal to 0.9, and the correlation coefficients are approximately greater than 0.6. The standard deviations range from 0.15 for pressure perturbations P to almost 1.0 for Sh and V_y.

The fields from experiment a3b3/t08q11 that have changed most significantly compared to experiment a2b3/t06q15 and the reference experiment are u, v, and V_x. For these fields, the RMS differences are *decreased* compared to experiment a2b3/t06q15 (the head of the arrow lies closer to the reference point than the tail), the amplitudes of the variations are *reduced* compared those of experiment a2b3/t06q15, and the correlations are either nearly zero (0.08 for v), still positive but reduced (.7 for u), or unchanged (-0.4 for V_x).

The Taylor Diagram based on averages of surface–only variables over the burning area for experiments a1b3/t01q15, a2b3/t06q15, and a3b3/t08q11 is given in Fig. 2. Fig. 2 shows that fields CI, CL, CS, GL, and GS from experiments a2b3/t06q15 and a2b3/t08q11 have the same amplitude of variations compared to the reference and are nearly in phase. The fields from experiments a2b3/t06q15 and a2b3/t08q11 that have changed somewhat compared to the reference are GI and SR. The arrows are oriented such that the variances are *smaller* in experiment a3b3/t08q11 compared to experiment a2b3/t06q15. The correlation coefficient for the fire spread rate SR has decreased somewhat in experiment a3b3/t08q11 compared to experiment a2b3/t06q15. The RMS difference for GI has increased only slightly.

b. Experiment a3b3/t11q15 compared to experiments a2b3/t06q15 and a1b3/t01q15

Fig. 3 highlights the differences between model fire a2b3/t06q15, rated as a Haines Index 5, and model fire a3b3/t11q15, rated as a high-end Haines Index 6. The RMS differences of experiment a3b3/t11q15 are *substantially* larger compared to experiment a2b3/t06q15 (the heads of arrows lie further away from the reference point than tails), with especially dramatic changes in u, v, V_y and V_x (very long arrow lengths). The variances in amplitude in experiment a3b3/t11q15 are increased greatly compared to the variances in amplitude in experiment

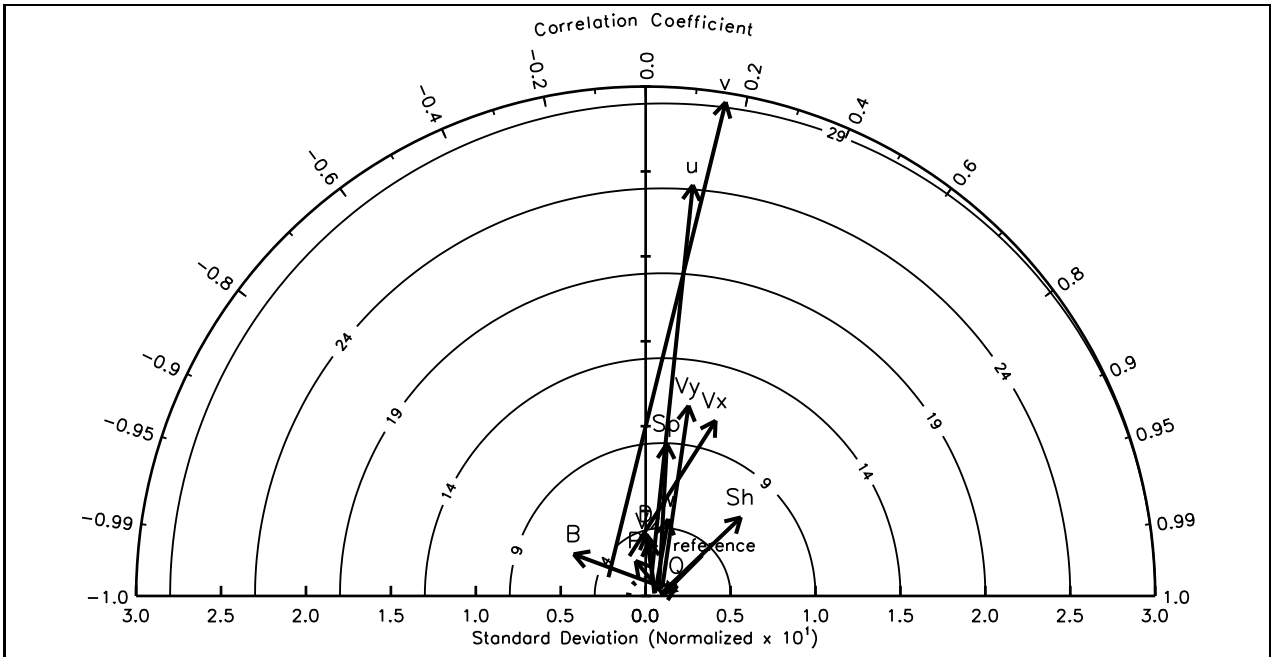

Fig. 3 Changes in pattern statistics between experiments a3b3/t11q15 and a2b3/t06q15. The statistics for experiment a2b3/t06q15 are plotted at the tail of the arrows, and the statistics for experiment a3b3/t11q15 at the head of the arrows. The fields shown are the same as those in Fig. 1.

a2b3/t06q15. For most fields the correlation between experiment a3b3/t11q15 and the reference is extremely poor (correlation coefficients approximately less than 0.4). The RMS differences range from 2.6 for P to 30.0 for v, and the standard deviations range from 2.2 for P to approximately 30.0 for u and v. The only field whose Taylor statistics change only moderately is Q (the shortest arrow length). In experiment a3b3/t11q15, the Q RMS difference is 1.0, the variance in amplitude is increased to 1.9, and the correlation coefficient remains nearly 1.00.

The Taylor diagram based on averages of surface–only variables over the burning area for experiments a1b3/t01q15, a2b3/t06q15, and a3b3/t11q15 is given in Fig. 4. The RMS differences for experiment a3b3/t11q15 are greatly increased compared to experiment a2b3/t06q15 (arrows point away from the reference point) for all fields, where the most obvious changes in the Taylor statistics are for fields CI, GI, and SR. The large and simultaneous change in the Taylor statistics for SR, GI, and CI, means that model fire a3b3/t11q15 experienced crowning. Examination of the data (not shown) confirms that at approximately 30 minutes into the simulation, model fire a3b3/t11q15 had a sudden and substantial increase in GI, SR, and CI that lasted for approximately 6 minutes.

5. DISCUSSION & CONCLUSIONS

Taylor statistics for experiments a1b3/t01q15 and a2b3/t06q15 show that most of the fields do not change significantly (i.e., w, P, B, Q, V_y, V_z, Sh, Sp, D) as low–level atmospheric stability is decreased. The correlation between most fields is relatively high, and many fields that might be expected to become more variant with decreased atmospheric stability (i.e., w, Sp, u, V_z, D) show an overall *reduction* in the amplitude of the variations. For a few fields (Q, P, Sh) there appears to be little or no statistical difference between experiments a1b3/t01q15 and a2b3/t06q15, despite the initial low–level environmental atmospheric stability in a2b3/t06q15 being less than that in a1b3/t01q15. A few fields (u, V_x and v) do have moderate statistical differences. Fields V_x and v are both poorly correlated and have differences in the amplitude of variations. Experiment a1b3/t01q15 is rated as a Haines Index 4, which indicates a low potential for severe fire behavior. Experiment a2b3/t06q15 is rated as a Haines Index 5, which indicates a moderate potential for severe fire behavior. What these statistics suggest is that for fires rated as a Haines Index 5 or lower, the atmospheric stability is not the deciding factor for severe fire risk within the first hour of burn when the initial environmental conditions include low wind speeds (3 m s^{-1}) with no vertical

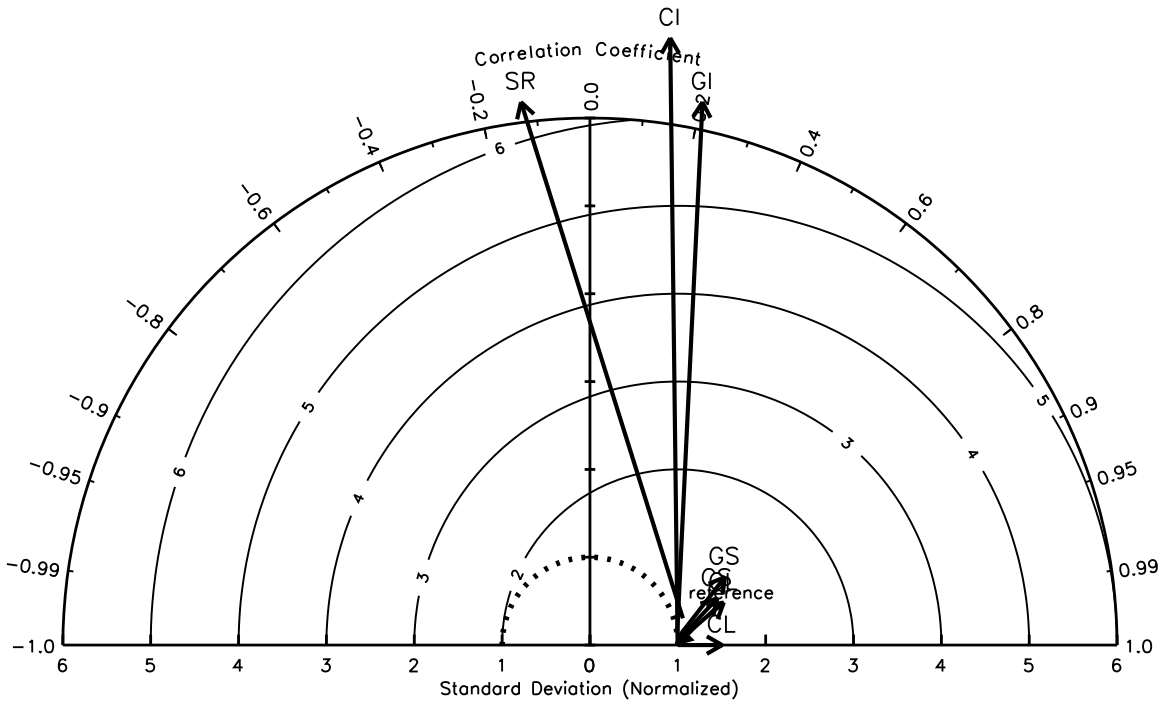

Fig. 4 Changes in normalized pattern statistics between experiments a2b3/t06q15 and a3b3/t11q15. Statistics for experiment a2b3/t06q15 are plotted at the tails of arrows, and the statistics for experiment a3b3/t11q15 are plotted at the heads of arrows. The RMS error and standard deviations are normalized by the standard deviation of each field from the reference experiment a1b3/t01q15 before plotting. The fields shown are the same as those in Fig. 2.

wind shear and no topography.

In marked contrast, the Taylor statistics for experiment a3b3/t11q15 show dramatic changes in all fields compared to experiments a1b3/t01q15 and a2b3/t06q15. The amplitude of variations has increased ten-fold, and the majority of fields show greatly reduced correlation with the reference experiment a1b3/t01q15 and experiment a2b3/t06q15. Only experiment a3b3/t11q15, rated as an upper–end Haines Index 6, responded strongly to the ambient atmospheric stability. The analysis showed the development of a large convection column, high rates of spread or acceleration of the fire front, increased fire intensity from ground and canopy fuel, and finally crowning. What the statistics suggest is that for this fire atmospheric stability is the deciding factor for severe fire risk. The statistics also suggest that there is a substantial range of fire behavior for fires rated as a Haines Index 6 (i.e., as illustrated by results from experiment a3b3/t06q15 and a3b3/t11q15). This implies that Index 6 should be refined, i.e., further divided into sub–indexes, for it to be a more accurate predictor of severe fire risk.

6. REFERENCES

Brotak, E. A., and W. E. Reifsnyder, 1977: Predicting major wildland fire occurrence. Fire Management Notes, **38**, Number 2. U.S. Dept. of Agriculture Forest Service.

Clark, T., M. A. Jenkins, J. Coen, & D. Packham, 1996: A coupled atmospheric-fire model: Convective feedback on fire line dynamics. *J. Appl. Meteor.*, **35**, 875-901.

Clark, T. L., M. A. Jenkins, J. Coen, and D. Packham, 1996: A coupled atmospheric-fire model: Role of the convective Froude number and dynamic fingering at the fire line. *International J. of Wildland Fire*, **6(4)**, 177-190.

Coen, J. L., and T. L. Clark, 2000: Coupled atmosphere–fire model dynamics of a fire line crossing a hill. *Preprints* of Third Symposium on Fire and Forest Meteorology, Amer. Meteor. Soc. 80th Annual Meeting, Los Angeles, CA, 7–10.

Haines, D. A., 1998: A lower atmospheric severity index for wildfires. *National Weather Digest*, **13**,

23–27.

Hirsch, K. G., 1996: Canadian forest fire behavior prediction (FBP) system: user's guide. Special Report 7. Canadian Forest Service, Northwest Region, Northern Foresty Centre. 122 pp.

Potter, B. E., 1996: Atmospheric properties associated with large wildfires. *International J. of Wildland Fire*, 6, **2**, 71–76.

Taylor, K. E., 2001: Summarizing multiple aspects of model performance in a single diagram. *J. Geophys. Res.*, **106**, 7183–7192.

Werth, J, and R. Ochoa, 1993: The evaluation of Idaho wildfire growth using the Haines Index. *Weather and Forecasting*, **8**(2), 223–234.